Global distribution of seamounts from ship-track bathymetry data

J. K. Hillier[1] and A. B. Watts[2]

[1]   The distribution of submarine volcanoes, or seamounts, reflects melting within the Earth and how the magma generated ascends through the overlying lithosphere. Globally (±60° latitude), we use bathymetry data acquired along 39.5×10^6 km of ship tracks to find 201,055 probable seamounts, an order of magnitude more than previous counts across a wider height-range ($0.1 < h < 6.7$ km). In the North Pacific, seamounts' spatial distribution substantially reflects ridge-crest conditions, variable on timescales of 10 s of Ma and along-ridge distances of ~1,000 km, rather than intra-plate hot-spot related volcanic activity. In the Atlantic, volcano numbers decrease, somewhat counter-intuitively, towards Iceland suggesting that abundant under-ridge melt may deter the formation of isolated volcanoes. Neither previously used empirical curve (exponential or power-law) describes the true size-frequency distribution of seamounts. Nevertheless, we predict $39 \pm 1 \times 10^3$ large seamounts ($h > 1$ km), implying that ~24,000 (60%) remain to be discovered. **Citation:** Hillier, J. K., and A. B. Watts (2007), Global distribution of seamounts from ship-track bathymetry data, *Geophys. Res. Lett.*, *34*, L13304, doi:10.1029/2007GL029874.

1.   Introduction

[2]   Seamounts reflect processes governing the generation and ascent of magma. So, the quantification of submarine volcanism has long been of geological interest. Sparse ship track data, however, hinders accurate quantification of the number, size, and location of seamounts. The method used to estimate true numbers is critical. Range of edifice height, h, and quantity of data studied are also issues as illustrated chronologically below by selected key papers on the best-studied Pacific Ocean.

[3]   *Menard* [1959] counted ~1000 'large' Pacific seamounts ($h > 1$ km) on 0.5×10^6 km of bathymetric profiles. Extrapolating roughly, to account for incomplete data, he estimated ~10^4 seamounts exist.

[4]   *Jordan et al.* [1983] found 331 seamounts from 0.044×10^6 km of single beam echo-sounder profiles of the East Pacific Rise (EPR). They formalised a statistical extrapolation to estimate true densities (number per 10^6 km²). Their usable seamounts ($0.3 < h < 1.5$ km) predict $3-5 \times 10^4$ large Pacific seamounts. The statistics assumed an exponential size-frequency distribution.

[5]   *Smith and Jordan* [1987, 1988] debated the appropriate form of the size-frequency distribution. 1,118 Pacific seamounts ($0.4 < h < 2.5$ km) found in 0.16×10^6 km of single beam data were compared with 186 seamounts ($0.1 < h < 1.1$ km) found in a smaller, nearby, area fully covered by swath bathymetry data. The comparison indicates that the exponential model may only be valid within a restricted height range. Furthermore, a power-law form is tested and rejected.

[6]   In contrast, *Abers et al.* [1988] analysed 382 seamounts ($0.1 < h < 1.1$ km) from swath bathymetry and found both power-law and exponential descriptions adequate. They also noted that, for large seamounts ($h > 1$ km), their exponential distribution under-predicts the single beam count whilst the power-law distribution over-predicts. Scaled up, their exponential and power-law distributions predict 10,000 and 400,000 large Pacific seamounts respectively.

[7]   Satellite altimetry has complete spatial coverage, so analysis of these data [*Wessel and Lyons*, 1997; *Wessel*, 2001] has yielded the largest number of Pacific seamounts to date; 8,882 ($h > $ ~2 km). Using a power-law ~70,000 large seamounts were predicted.

[8]   To better understand the world's oceanic volcano population this paper compiles seamounts in 39.5×10^6 km of NGDC archived single-beam ship bathymetry. Spatial distributions are analysed. Then, since probable seamounts are recovered across their entire height-range, size-frequency distributions can be assessed. Finally, an appropriate method to estimate true seamount numbers is developed.

2.   Method

[9]   Seamounts are isolated using the MiMIC algorithm [*Hillier and Watts*, 2004]. MiMIC reproducibly simulates the manual drawing of a line underneath seafloor features of a seamount-like morphology on a bathymetric profile. These 'seamounts' are most likely to be off-summit tra-verses of submarine volcanoes [*Batiza*, 1982; *Abers et al.*, 1988; *Wessel*, 2001; *Koppers et al.*, 2003]. Non-volcanic edifices cause the number of volcanoes of height h to be overestimated, whilst the sampling causes underestimation. Seamounts are approximated as flat-topped cones so that, where multiple ship-tracks traverse the same seamount, the tallest section, presumably the nearest to the summit and closest to the true seamount height, is selected [*Hillier*, 2006]. Artifacts due, for example, to wrap errors [*Smith*, 1993], and track geometry are eliminated [*Hillier*, 2006]. Also, features with slopes >20° are treated as artifacts, consistent swath bathymetry observations [*Abers et al.*, 1988; *Smith and Cann*, 1992].

3.   Spatial Distribution

[10]   201,055 seamounts ($h > 0.1$ km) are isolated, an order of magnitude more than counts based on bathymetric charts [*Menard*, 1964; *Batiza*, 1982; *Marova*, 2002] and satellite altimetry [e.g., *Wessel*, 2001]. Figure 1 shows the distribution of 46,792 seamounts with $h > 0.5$ km derived

[1]Department of Earth Science, University of Cambridge, Cambridge, UK.

[2]Department of Earth Science, University of Oxford, Oxford, UK.

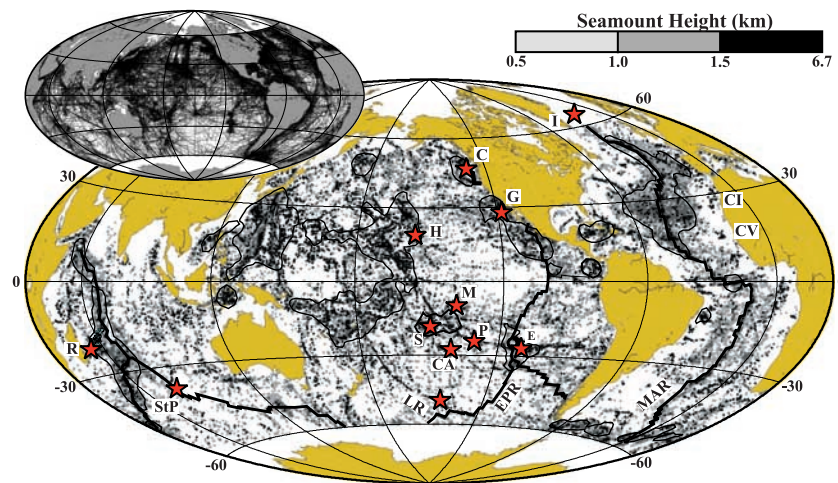**Figure 1.** Spatial distribution of seamounts (dots): $0.5 < h < 1$ km, light grey (n = 32,211); $1 < h < 1.5$ km, grey (n = 8,436); $h > 1.5$ km, black (n = 6,145). Thin black line delimits areas of high seamount density (defined as 75 seamounts of $h > 1$ km per 10^6 km^2 within a 500 km radius). Thick black lines are spreading ridges: EPR, East Pacific Rise; MAR, Mid-Atlantic Ridge. Stars locate commonly cited 'hot spots': CA, Cook-Austral; CI, Canary; CV, Cape Verde; C, Cobb; E, Easter; G, Guadalupe; H, Hawaii; I, Iceland; LR, Louisville; M, Marquesas; P, Pitcairn; R, Reunion; S, Society; StP, St Paul's. Inset is coverage of bathymetric data measured along ship-tracks. For data (Longitude, Latitude, height, volume) see auxiliary material.

using the MiMIC and global ship track data[1]. Darker shades indicate larger seamounts.

[11] The distribution of very large seamounts ($h > 1.5$ km) is consistent with previous map compilations [e.g., *Menard*, 1964; *Craig and Sandwell*, 1988; *Marova*, 2002]. Quantitatively, areas containing high spatial densities of seamounts (delimited by thin black lines) agree well with those of *Wessel and Lyons* [1997]. Also, for instance, the majority (58%) of 'large' seamounts ($h > 1$ km) still occur in the Pacific [*Marova*, 2002; *Wessel*, 2001]. However, with MiMIC 'small' ($h < 1$ km) seamounts can also be examined.

[12] In the well-surveyed northern hemisphere, the distribution of small seamounts is probably reliable. In the southern oceans, data are sparse and align along ship tracks. *Menard* [1959], however, had a very sparse data set, yet it has been proved to be representative of the distribution of large seamounts. We therefore believe the whole first-order pattern of small seamounts in Figure 1 to be informative, even before data coverage is corrected for.

[13] An absence of small seamounts at the margins of the Atlantic is due to the thick sediment cover. Small seamounts are associated with larger volcanic edifices (e.g. the Guadalupe hot-spot) and conversely may be sparse in other regions (e.g. the equatorial central Pacific). There are also large variations in the concentration of small seamounts along the mid-ocean crests.

[14] In the North Atlantic, seamounts of $h < 1.5$ km increase in density from the equator, peak between 20–30°N, and then decline across the Charlie-Gibbs Fracture Zone towards Iceland. This trend is not obviously related to fracture zone spacing, data coverage, on-ridge sediment thickness, or spreading rate [*Scheirer and MacDonald*, 1995]. Neither can it be attributed to and abyssal hill topography, which is <700 m in amplitude [*Bohnensteihl and Kleinrock*, 2000]. Therefore, the decline in seamounts

numbers as the ridge shallows is probably real, which is perhaps surprising since Iceland is a hotspot, but is in accord with observations at Galapagos [*Detrick et al.*, 2002; *Behn et al.*, 2004]. Abnormally abundant under-ridge melt may generally, therefore, deter the formation of isolated volcanoes.

[15] In the North Pacific, the number and density (no. per 10^6 km^2) of seamounts on Figure 1 progressively decreases with increasing crustal age from 0–80 Ma (even if data coverage is later considered). The decrease dictates that volcanic emplacement is everywhere not steady-state (constant through time) as previously advocated [*Batiza*, 1981, 1982; *Smith and Jordan*, 1988; *Marova*, 2002]. Alternatively, steadily increasing near-ridge seamount production over the last 80 Ma may have occurred. If so, the decrease is consistent with a scenario where, in accord with studies at the EPR [*Abers et al.*, 1988; *Scheirer and MacDonald*, 1995; *Scheirer et al.*, 1996] (seafloor < a few Ma), seamounts must dominantly form quickly on young seafloor, the smaller the younger. Here, however, the model is extended to much larger length scales and periods of time. Consequently, the decrease suggests that seamount distribution substantially reflects ridge crest conditions, variable on timescales of 10 s of Ma and along-ridge distances of ~1,000 km, rather than intra-plate hot-spot related volcanic activity. In a third, less likely, case all volcanism may be recent. In either scenario, the decrease is direct, large-scale evidence that old lithosphere is more of a barrier to melt than young lithosphere.

[16] Globally, several quanitfications of the measured seamount population provide an interesting comparison with literature values. In these calculations, total area of oceanic seafloor is 371×10^6 km^2 calculated as a sum of $0.1 \times 0.1°$ areas of depth >500 m, radial symmetry is assumed for seamounts, and estimates are minima in the respect that only measured edifices are used.

[17] Numerically then, the footprints of the small seamounts measured cover 45.9×10^6 km^2 of oceanic seafloor,
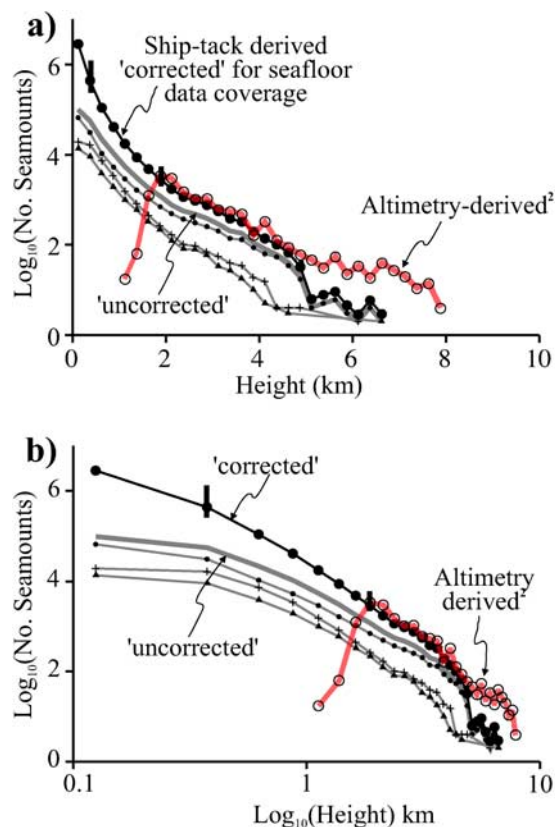
Figure 2. Linear-log and log-log plots of the size-frequency distribution of global seamounts corrected (black circles) and uncorrected (grey line) for incomplete seafloor data coverage. Counts are incremental (i.e. number in each 0.25 km bin) and plotted centred within the bins. Vertical bars at h values of 0.375, 1.875 and 4.875 km illustrate error in correction from varying r/h across the entire plausible range $0.07-0.36$ (i.e. slopes $4-20°$). Small symbols joined by grey lines are Pacific (circles), Indian (triangles) and Atlantic (crosses) seamounts. Bin for smallest heights contains $0.1 < h < 0.25$ only. Open circles are altimetry-derived detections of large seamounts [*Wessel*, 2001]. Note, maximum abyssal hill heights; Pacific 0.2 km [e.g., *Menard and Mammerickx*, 1967], Atlantic 0.7 km [*Bohnensteihl and Kleinrock*, 2000].

or 12.4%, which is greater than 7.2% for large seamounts and previous total estimates of 6% [*Jordan et al.*, 1983; *Scheirer and MacDonald*, 1995]. Together, tall seamounts have a volume of 21.5×10^6 km^3 equivalent to a layer 58.0 m thick across the ocean basins, between previous estimates of $27-110$ m [*Jordan et al.*, 1983; *Marova*, 2002; *Wessel*, 2001]. The $0.5-1$ km height interval, however, contains the largest volume of any 500 m bin. So, small seamounts appear important, perhaps dominant.

4. Size-Frequency Distribution

[18] Seamount populations have also been described in terms of size-frequency distributions, and represented by exponential [e.g., *Abers et al.*, 1988; *Wessel and Lyons*, 1997] ($\nu(H) = \nu_0 e^{-\beta H}$) and power-law [e.g. *Smith and Jordan*, 1988; *Wessel*, 2001] ($\nu(H) = \nu_1 H^{-\gamma}$) expressions.

Here, H is seamount height, $\nu(H)$ is the number of seamounts in a height bin, and β is the slope in linear-log space. In addition, 'cumulative' expressions have been used
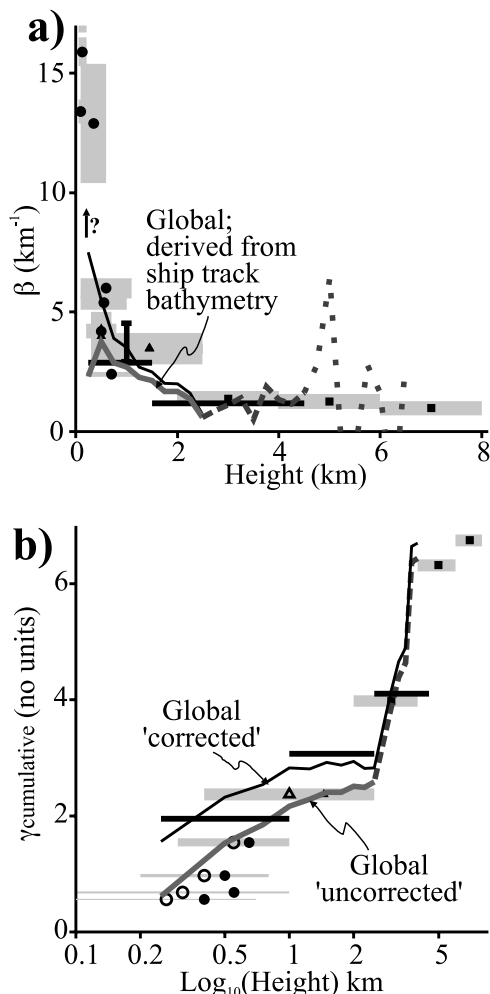

Figure 3. Slopes of (a) exponential and (b) cumulative power-law distributions. $\gamma_{cumulative}$ is used for comparison with literature values (grey boxes). Box widths represent the height range of data fitted, and height representing estimated error in slope. Circles centred in boxes are estimates from multi-beam data [*Smith and Jordan*, 1987; *Abers et al.*, 1988; *Bemis and Smith*, 1993; *Kleinrock et al.*, 1994; *Scheirer and MacDonald*, 1995; *Scheirer et al.*, 1996], triangles from single-beam [*Jordan et al.*, 1983; *Smith and Jordan*, 1987, 1988; *Bemis and Smith*, 1993], squares are altimetry-derived [*Wessel*, 2001]. Values for *Wessel* [2001] are 'Ordinary Least Squares' fits to their incremental data; errors are nominal. Horizontal black bars are OLS fits to our data. Grey line is gradient between consecutive points for our data: dashed and dotted sections indicate increasing uncertainty with decreasing count. Thin black line shows effect of correction for incomplete seafloor sampling. β is little affected by W (β varies $\pm \sim 0.1$ for W varied to 100 m and 500 m), as is γ (γ varies $\pm \sim 0.1$ for W similarly varied). Point relating to smallest seamount would increase if $h < 0.1$ km could be included. In a) Vertical black bar spans β for 8 regions across the Pacific determined by *Smith and Jordan* [1988] (single-beam, $0.4 < h < 1.6$ km).

Table 1. Number of Seamounts Within Height Bins[a]

	Height, km			
Ocean	$0.5 < h < 1$	$1 < h < 1.5$	$h > 1.5$	Total ($h > 0.1$)
Indian[b]	5,705 (35,238)	1,571 (5,985)	973 (2,647)	30,873 (729,070)
Pacific[c]	15,925 (73,942)	4,519 (13,805)	3,874 (8,654)	120,456 (2,140,063)
Atlantic[d]	10,581 (42,647)	2,346 (6,291)	1,298 (2,694)	49,726 (608,270)
Global Total	32,211 (151,827)	8,436 (26,081)	6,145 (13,995)	201,055 (3,477,403)
Altimetry Derived[e]	0	170	14,164	14,334

[a]Counts corrected for seafloor data coverage are in brackets.
[b]$20-130°E$, -60 to $20°N$ (no ocean north of this). 689 ship tracks - 5.8×10^6 km.
[c]$130-290°E$, $\pm60°N$. 3098 tracks - 21.7×10^6 km.
[d]$70°W-20°E$, $\pm60°N$. 1704 tracks - 12.0×10^6 km.
[e]*Wessel* [2001] $\pm60°N$.

[Jordan et al., 1983; Smith and Jordan, 1987, 1988; Smith and Cann, 1992; Bemis and Smith, 1993; Kleinrock et al., 1994; Scheirer and MacDonald, 1995] where $\nu(H)$ is the number of seamounts of $h \geq H$, and $\beta_{cumulative} = \beta$. In the case of the power-law [Smith and Jordan, 1987, 1988; Abers et al., 1988; Main, 2000] slope in log-log space, $\gamma_{cumulative}$, is $\simeq \gamma - 1$.

[19] The range in height, h, of our seamounts ($0.1 < h < 6.7$ km) exceeds that of previous studies allowing us to comment on which analytical approximation, if any, is valid.

[20] Figure 2 shows both linear-log and log-log plots of the global size-frequency distribution of seamounts (i.e., the number in a bin of width W). The figure shows that neither the global data (grey solid line) nor the data for each ocean (small symbols) form a straight line on either the linear-log or the log-log plot. This demonstrates that no single exponential or power-law curve can describe seamount heights over the whole size range.

[21] This result is significant in that an analytical form is required in order to statistically [Jordan et al., 1983] estimate the true numbers of seamounts from a data set that is limited in coverage and therefore the height of recovered features. Extrapolating with an exponential (linear approximation to concave data) will always under-predict true numbers, whilst the power-law (linear approximation to convex data) will over-predict. Locally, these predictive biases have been attributed to 'some sort of sampling bias' associated with feature recognition [Smith and Jordan, 1988], regional seamount heterogeneities [Smith and Jordan, 1987, 1988], distinct height-based seamount populations [Bemis and Smith, 1993], and the possibility that the exponential model may only be locally valid within a particular height range [Smith and Jordan, 1987, 1988; Abers et al., 1988; Bemis and Smith, 1993]. We, however, can assert that variation with h is a real, pervasive, and important feature of the distribution.

[22] Figure 3 plots the gradients, β and $\gamma_{cumulative}$, of our global curve (solid grey line, Figure 2). The figure shows a progressive decrease of β, and increase in $\gamma_{cumulative}$ with increasing height. These results agree with estimates derived from multi-beam (circles), single beam echo sounder (triangles), and satellite altimetry (squares). Together, the data show that the trends in β and γ are continuous for all seamount heights and invariant to methodological details.

[23] Despite the lack, therefore, of a mathematically simple approximation (exponential or power-law), we formulate a simple geometrical correction for seafloor data

coverage to predict the true seamount population. Complexity is minimized. Firstly, radius, r, is related to measured h by $h = 0.14r$ where 0.14 is the mean h/r of our measured data ($1 < h < 4$ km). Then, coverage as a function of h, is calculated as the fraction, f, of spatial bins ($r \times r$) containing data with a median depth >500 m. The correction is then $1/f$. For example, with $f = 0.1$, the number of seamounts in a height bin would be multiplied by 10.

[24] Note that f would have to be systematically in error by $\sim \times 100$ across seamount heights to affect the conclusions about size-frequency distributions above. Conical seamounts sampled by random traverses, for instance, would have h underestimated by the same proportion whatever h is. So, the correction substantially circumvents assumptions in the statistical analyses that seamounts are randomly distributed in space, do not overlap, and are on linear tracks [Jordan et al., 1983].

[25] Absolute corrected numbers are justified by their close agreement with the large seamounts recovered from satellite altimetry [Wessel, 2001] (Figure 2, open circles), which has complete spatial coverage. The agreement is probably assisted because when sampling underestimates true h, thus r, $1/f$ is overestimated, effects which cancel when estimating $\nu(H)$. Differences between the two distributions arise because the satellite-derived gravity data is apparently able to recover sub-aerial volcanic islands (296 features h $5-8$ km) inaccessible to ships, but does not have the resolution to recover seamounts of $h < 2$ km. We can, however, use ship track data to estimate the number of these small seamounts that remain to be discovered.

[26] Table 1 summarises the number of seamounts within the height bands used in Figure 1 and counts corrected for data coverage. Wessel's [2001] 14,164 seamounts with $h > 1.5$ km compare well to our 13,995, although we predict $\sim 25\%$ fewer seamounts of $1.75 \leq h \leq 5$ km. In the Pacific we expect $\sim 22,000$ large ($h > 1$ km) volcanoes, and $39 \pm 1 \times 10^3$ globally, the accuracy estimated from the variance of predictions using a randomly selected 10% of seamounts. Height measurement error will increase this variability and changing r/h by ± 0.04 (slope $\sim 8 \pm 3°$) alters estimates by $\sim \pm 7,000$. However, we believe the result is a significant constraint upon the current estimates that range from 15,000 [Marova, 2002] to 100,000 [Wessel, 2001]. More speculatively, we expect around 3 million seamounts of $h > 0.1$ km.

References

Abers, G. A., B. Parsons, and J. K. Weissel (1988), Seamount abundances and distributions in the southeast Pacific, *Earth Planet. Sci. Lett.*, *87*, 137–151.

Batiza, R. (1981), Lithospheric age dependence of off-ridge volcano production in the North Pacific, *Geophys. Res. Lett.*, *8*, 853–856.

Batiza, R. (1982), Abundances, distribution and sizes of volcanoes in the Pacific Ocean, *Earth Planet. Sci. Lett.*, *60*, 195–206.

Behn, M. D., J. M. Sinton, and R. S. Detrick (2004), Effect of the Galapagos hotspot on seafloor volcanism along the Galapagos Spreading Centre, *Earth Planet. Sci. Lett.*, *217*, 331–347.

Bemis, K. G., and D. K. Smith (1993), Production of small volcanoes in the Superswell region of the South Pacific, *Earth Planet. Sci. Lett.*, *118*, 251–262.

Bohnensteihl, D. R., and M. C. Kleinrock (2000), Spreading-rate dependence in the displacement-length ratios of abyssal hill faults at mid-ocean ridges, *Geology*, *28*, 395–398.

Craig, C. H., and D. T. Sandwell (1988), Global distribution of seamounts from Seasat profiles, *J. Geophys. Res.*, *93*, 10,408–10,420.

Detrick, R. S., et al. (2002), Manifestations of plume-ridge interaction along the Galapagos Spreading Centre, *Geochem. Geophys. Geosyst.*, *3*(10), 8501, doi:10.1029/2002GC000350.

Hillier, J. K. (2006), Pacific seamount volcanism in space and time, *Geophys. J. Int.*, *168*, 877–889, doi:10.1111/j.1365-246-X.2006.03250.x.

Hillier, J. K., and A. B. Watts (2004), "Plate-like" subsidence of the East Pacific rise–South Pacific superswell system, *J. Geophys. Res.*, *109*, B10102, doi:10.1029/2004JB003041.

Jordan, T. H., H. W. Menard, and D. K. Smith (1983), Density and size distribution of seamounts in the eastern Pacific, *J. Geophys. Res.*, *88*, 10,508–10,518.

Kleinrock, M. C., B. A. Brooks, and D. K. Smith (1994), Construction and destruction of volcanic knobs at the Coca-Nazca spreading system near 95°W, *Geophys. Res. Lett.*, *21*, 2307–2310.

Koppers, A. A. P., H. Staudigel, M. S. Pringle, and J. R. Wijbrans (2003), Short-lived and discontinuous intraplate volcanism in the South Pacific: Hot spots or extensional volcanism?, *Geochem. Geophys. Geosyst.*, *4*(10), 1089, doi:10.1029/2003GC000533.

Main, I. (2000), Apparent breaks in scaling in the earthquake cumulative frequency-magnitude distribution: Fact of artifact, *Bull. Seismol. Soc. Am.*, *90*, 86–97.

Marova, N. A. (2002), Seamounts of the world ocean, *Oceanology*, *42*(3), 409–413.

Menard, H. W. (1959), Geology of the Pacific seafloor, *Experimentia*, *15*, 205–244.

Menard, H. W. (1964), *Marine Geology of the Pacific*, 271 pp., McGraw-Hill, New York.

Menard, H. W., and J. Mammerickx (1967), Abyssal hills, magnetic anomalies and the East Pacific Rise, *Earth Planet. Sci. Lett.*, *2*, 465–472.

Scheirer, D. S., and K. C. MacDonald (1995), Near-axis seamounts on the flanks of the East Pacific Rise, *J. Geophys. Res.*, *100*, 2239–2259.

Scheirer, D. S., K. C. MacDonald, and D. W. Forsyth (1996), Abundant seamounts of the Rano Rahi seamount field near the southern EPR, *Mar. Geophys. Res.*, *18*, 13–52.

Smith, D. K., and J. R. Cann (1992), The role of seamount volcanism in crustal construction at the Mid-Atlantic Ridge, *J. Geophys. Res.*, *97*, 1645–1658.

Smith, D. K., and T. H. Jordan (1987), The size distribution of Pacific seamounts, *Geophys. Res. Lett.*, *14*, 1119–1122.

Smith, D. K., and T. H. Jordan (1988), Seamount statistics in the Pacific Ocean, *J. Geophys. Res.*, *93*, 2899–2918.

Smith, W. (1993), On the accuracy of digital bathymetric data, *J. Geophys. Res.*, *98*, 9591–9603.

Wessel, P. (2001), Global distribution of seamounts inferred from gridded Geosat/ERS-1 altimetry, *J. Geophys. Res.*, *106*, 19,431–19,441.

Wessel, P., and S. Lyons (1997), Distribution of large Pacific seamounts from Geosat/ERS-1, *J. Geophys. Res.*, *102*, 22,459–22,475.

———————————

J. K. Hillier, Department of Earth Science, University of Cambridge, Downing Street, Cambridge CB2 3EQ, UK. (jkh34@cam.ac.uk)

A. B. Watts, Department of Earth Science, University of Oxford, Parks Road, OX3 1PR Oxford, UK. (tony.watts@earth.ox.ac.uk)